THIRD AFOSR INTERNATIONAL CONFERENCE ON DNS AND LES, UNIVERSITY OF TEXAS AT ARLINGTON, TEXAS, U.S.A., AUGUST 5-9, 2001

LARGE-EDDY SIMULATION OF THE FLOW AROUND A SIMPLIFIED BUS

SINIŠA KRAJNOVIĆ AND LARS DAVIDSON
Department of Thermo and Fluid Dynamics
Chalmers University of Technology
SE-412 96 Göteborg, Sweden
sinisa@tfd.chalmers.se

Abstract. Two large eddy simulations of the flow past a bus-like vehicle body were made and the results are compared with experimental data [3]. The effect of the near wall resolution and the modeling of the unresolved coherent structures in the near wall flow were studied. It was determined that, although the wall functions are inadequate to represent the thin vortices close to the wall, their use leads to results in a near wake region that are similar to those in the simulation with a sufficient wall normal resolution. This study indicates that the wall normal resolution has little influence on the pressure coefficient at the rear face.

1. Introduction

The drag forces of importance to the vehicle designer are dominated primary by the wake forces. Thus the prediction of the pressure coefficient at the rear of the vehicle is of great importance. Although the RANS simulations have been successful in predicting many parts of the flow around vehicles, they have failed to predict the effects of the unsteady wake on the body. It is believed than an unsteady simulation such as large eddy simulation (LES) will have greater success than RANS in predicting the pressure at the rear of the vehicles and give better insight into the flow around these bodies. Large eddy simulation has already been applied to various bluff body flows. Early bluff body LES were made of the flow around a surface-mounted cube and a rectangular cylinder. These flows are characterized by the separations defined by the sharp edges of the obstacle. Breuer [2] made LES of the flow around a circular cylinder at Reynolds number 140000 ba-

sed on the free stream velocity and cylinder diameter. This flow involves transition and a very thin separation shear layer, which makes LES very challenging. While the drag generation on the two-dimensional cylinders is dominated by the regular shedding of intense vortices, the flow around highly three-dimensional vehicles is highly irregular [1]. The cylinders studied in these LES were isolated (i.e. not in the vicinity of the ground plane) and the cube was mounted on the ground, whereas the vehicle body is in the vicinity of the ground. The vicinity of the ground forces the stagnation point away from the center of the front face towards the bottom of the body, which produces different flows on the top and bottom surfaces and thus generates a lift force [1]. All these factors make these LES of limited relevance to flow past a vehicle. Krajnović and Davidson [5] recently presented LES of the flow around a bus-like body where they modeled the coherent structures near the wall with wall functions. The shape and the ground clearance of this body are similar to the shape and clearance of the buses. This makes it an excellent test case for investigation of the applicability of LES in vehicle aerodynamics.

The long term goal of this study is to develop a LES that is able to simulate the flow around a vehicle. The main obstacle of a LES of this kind is the near wall resolution required to represent the vortex structures in the shear layer. The purpose of this paper is to present LES of the flow around a bus-like bluff body at $Re = 210000$. We compare two LES in which the near wall region was treated in different ways.

2. Subgrid-scale modeling and numerical method

The effect of the small scales, which appears in the subgrid-scale stress tensor in the filtered Navier-Stokes equations, is modeled using the Smagorinsky model. The Smagorinsky constant, C_s, equal to 0.1 is used in this work and the Van Driest damping function was used only in the $LES2$ simulation. The formation of a turbulent boundary layer in the experiment was ensured with boundary layer trip wires mounted at the front of the model. Because of this there is no laminar boundary layer on the body and the assumption of non zero SGS stresses used in our LES is thus correct. In the case of transition from laminar to turbulent flow on the body, some correction is needed to force SGS stresses to zero in the laminar region. An alternative is to use a different SGS model, e.g. the dynamic eddy viscosity model, in which the eddy viscosity vanishes in laminar flows.

Calculations are made with the CALC-BFC code. This is based on a 3-D finite volume method for solving the incompressible Navier-Stokes equations using a collocated grid arrangement. Both convective and viscous fluxes are approximated by central differences of second order accuracy. A

Crank-Nicolson second order scheme was used for time integration. The SIMPLEC algorithm was used for the pressure-velocity coupling. The code is parallelized with block decomposition and the PVM and MPI message passing systems [6].

3. Description of the geometry and numerical details

The geometry of the computational domain is given in Fig.1. A domain with an upstream length of $x_1/H = 8$, a downstream length of $x_2/H = 16$ and a span-wise width of $B = 5.92H$ was used for the simulation. The values of other geometrical quantities are $L = 0.46$ m, $H = 0.125$ m, $W = 0.125$ m, $S = 0.3075$ m, $R = 0.019$ m, $r = 0.0127$ m, $c = 0.01$ m and $C = 0.5$ m. The ground clearance of $c/H = 0.08$ is similar to the clearance ratio of buses. The Reynolds number $Re = U_\infty H/\nu$ was 210000 on the basis of the incoming mean velocity, U_∞, and the vehicle height, H. In the experimental set-up, the location of the front side relative to the inlet was 0.564 m and the distance from the test section exit to the back wall perpendicular to the flow was 1.854 m. A moving ground belt and boundary layer scoop were used to simulate the floor boundary condition and to minimize boundary layer effects. The cross-section of the tunnel test section, the ground clearance and the position of the model's cross-section with respect to the tunnel were identical in LES and the experimental set-up.

In the experiments of Duell and George [3], the inlet mean velocity was uniform within 1% and the average turbulent intensity was 0.3%. A uniform velocity profile constant in time was thus used as the inlet boundary condition in this work. The convective boundary condition $\frac{\partial u_i}{\partial t} + U_c \frac{\partial u_i}{\partial x} = 0$ was used at the downstream boundary. Here, U_c was set equal to the incoming mean velocity, U_∞. To simulate the moving ground, the velocity of the lower wall was set equal to U_∞. The lateral surfaces were treated as slip surfaces using symmetry conditions $\frac{\partial u}{\partial z} = \frac{\partial v}{\partial z} = w = 0$. The wall functions based on the 'instantaneous logarithmic law' are used at all walls in simulation $LES1$. We refer to Ref. [5] for the details of the implementation of the wall functions. In the $LES2$ simulation, no-slip boundary conditions were used on the wall. The homogeneous Neumann condition was used for the pressure at all boundaries.

The topology of the mesh consists of 24 blocks where one block forms an O grid. An additional larger bus surface was made for the outer surface of the O grid. The O grid with a thickness of 0.005 m was made between this surface and the surface of the vehicle body. The number of cells in the wall normal direction in the O grid was 10 in simulation $LES1$ and 30 in simulation $LES2$. The rest of the mesh was the same in both simulations. Meshes of 1.8 million and 2.1 million nodes were used in simulations $LES1$

and $LES2$, respectively. The time step was 2×10^{-4} in $LES1$ and 1×10^{-4} in $LES2$, giving a maximal CFL number of approximately 4.5. The CFL number was smaller than one in 98% of the cells. The averaging time in the simulation was $tU_\infty/H = 48$ (30000 time steps in $LES1$ and 60000 time steps in $LES2$). The computational cost using 24 SGI R10000 CPUs was $\simeq 600$ hours (elapsed time) for $LES1$ and 1200 hours for $LES2$.

4. Results

4.1. THE MEAN FLOW

Time-averaged velocities $\overline{V}_{eff} = \left(\langle\bar{u}\rangle_t{}^2 + \langle\bar{v}\rangle_t{}^2\right)^{1/2}$ are compared with hot wire anemometry experimental data in Fig. 2. Here, $\langle\bar{u}\rangle_t$ and $\langle\bar{v}\rangle_t$ are time-averaged resolved velocity components in the x and y directions obtained from LES. The agreement of LES results with experimental data is relatively good, and all the peaks and trends of the experimental profile are represented in the LES results. Although the two LES gave very similar velocity profiles, there are some differences, especially at position $x/H = 0.32$. The velocity profile in simulation $LES1$ is in better agreement at this location with the experimental data than is the one in $LES2$. In the experiments of Duell and George [3], the free stagnation point was assumed to be at $y = 0$. They plotted $\overline{V}_{eff}/U_\infty$ along the x-axis and used the local minimum as the indication of the free stagnation point. The distribution of the mean velocity components, $\langle\bar{u}\rangle_t/U_\infty$ and $\overline{V}_{eff}/U_\infty$, at $y = 0$ observed in our LES are plotted in Fig 3a. The recirculation length was found to be $X_r = 1.36H$ in $LES1$ and $X_r = 1.39H$ in $LES2$ using the local minimum of $\overline{V}_{eff}/U_\infty$. Using the intersection of $\langle\bar{u}\rangle_t/U_\infty$ with the x-axis, we found $X_r = 1.44H$ in $LES1$ and $X_r = 1.41H$ in $LES2$. This is larger than the $X_r = 1.1H$ measured in Duell and George's experiment [3]. The local minimum of $\overline{V}_{eff}/U_\infty$ in Fig. 3a is larger than zero, which indicates that the free stagnation point is not fixed. This finding agrees with experimental result [3]

The pressure coefficient at the rear face, $C_{p_{base}} = (p - p_\infty)/(0.5\rho U_\infty^2)$, in LES is computed and compared with the experimental data in Fig. 3b. It can be seen that the shape of the profile is the same as in the experiment, while the level of $C_{p_{base}}$ is over-predicted in both simulations. The integrated value of $C_{p_{base}}$ over the rear surface, $\overline{C}_{p_{base}}$, was -0.216 in the $LES1$ simulation and -0.224 in the $LES2$ simulation as compared to the experimental value of -0.286.

4.2. THE INSTANTANEOUS FLOW

The $C_{p_{base}}$ signal was Fourier transformed and a peak is found in the spectrum. The Strouhal number, $St = fH/U_\infty$, of this periodic component signal was 0.069 in simulation $LES1$, whereas two peaks were found in simulation $LES2$ corresponding to the non-dimensional frequencies of $St = 0.055$ and $St = 0.195$. This can be compared to the experimental value of 0.073.

The velocity signals for two points in the near wake were sampled and turbulent energy spectra computed. The selected points are located in the upper shear layer of the recirculation region and in the wake region close to the free stagnation point. The same points were chosen for the velocity signal sampling in the experiments of Duell and George [3]. The energy spectra of these signals exposed several dominant frequencies. Distinct peaks corresponding to the non dimensional frequencies of $St = 0.032$, $St = 0.21$ and $St = 0.29$ in simulation $LES1$ and 0.517, 1.079 and 1.323 in simulation $LES2$ were measured near the separation point. In the experiment, Duell and George [3] measured $St = 1.155$ at this position. The power density spectrum at the second point close to the free stagnation point has a peak at $St = 0.11$ in $LES1$ and $St = 0.472$ in $LES2$ as compared to the experimental value of $St = 0.155$.

4.3. THE FLOW STRUCTURES

The coherent structures were visualized and compared with the experimental observations. Simulation $LES2$ was found to be superior to $LES1$ in resolving the flow structures around the bus. The reason is that the near wall resolution of one wall unit in $LES2$ makes it possible to resolve these structures, whereas the wall functions used in $LES1$ are not able to reproduce the re-attachments and separations. The flow separates at the rounded leading edge in simulation $LES2$, similar to experimental observations, and forms the vortex on the roof (R) and two vortices on the lateral sides of the bus (L). These vortices can be seen in Figs. 4 and 5a. We calculated vortex cores using EnSight post-processing software and according to algorithms based on techniques outlined by Sujudi and Haimes [7]. Core segments are then used as emitters for the streamlines shown in Fig. 5a. This figure shows that the roof vortex (R) and the lateral vortices (L) end at the surface of the body and that they are connected with smaller vortices in between, over the rounded edges. This satisfies Helmholtz's second vortex theorem, which states that the vortices must end at a solid boundary, extend to infinity or be connected to each other. The trailing vortices (T) were predicted in both simulations (see Fig. 5 and Ref.[5]). The vortex shedding from the sharp rear edges of the model forms four straight vortices shown in Figs. 5b, 6b and 7b. Similar vortices were found in a study of the shedding from the

separation lines of discs and square plates [4]. Figures 6a and 7a show that the $LES1$ simulation failed to predict these vortices, again showing that wall functions are unable to deal with these coherent structures.

The experimental observation [3] of the strong ring-type vortex (W) was confirmed in LES1[5] and is shown in Fig. 5b in LES2. Although both simulations show two wake vortices, in agreement with experimental observations, there are evident differences in their size and the position of the foci (F1 and F2) and saddle point (SP). In agreement with experiments, the lower vortex is smaller than the upper one. Figure 6 shows that the position of the stagnation point on the rear face of the model is different between the two simulations. Similar differences between the two simulations were observed in plane $y = 0$ in Fig. 7. Asymmetry in the flow behind the body in Fig. 7 indicates strong vortex interaction in the spanwise direction, which increases the requirement of longer time averaging.

4.4. ACKNOWLEDGMENTS

This work was supported by NUTEK and the Volvo Car Corporation. Computer time on the SGI ORIGIN 2000 machines, provided by UNICC at Chalmers, is gratefully acknowledged.

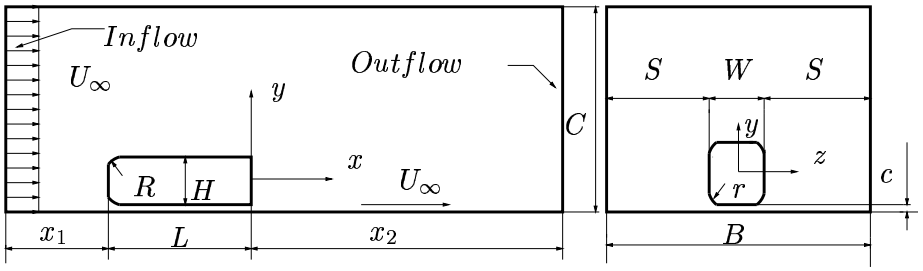

Figure 1. Geometry of the vehicle body and computational domain.

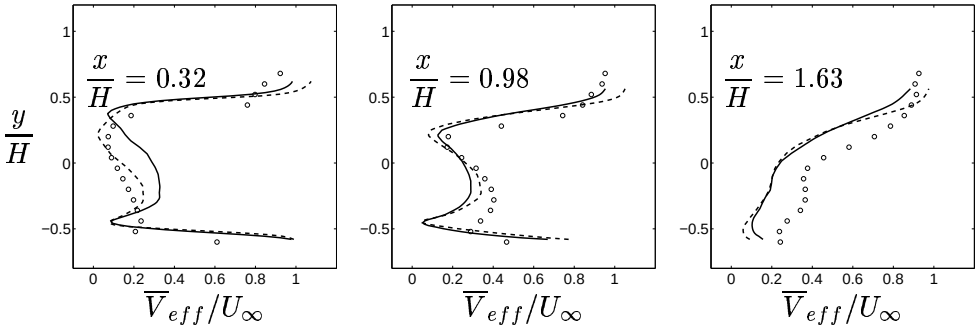

Figure 2. Time-averaged velocity profiles at three downstream locations at $z = 0$. $LES1$ (dashed line); $LES2$ (solid line); experiment (symbols).

References

1. P. W. Bearman. Review - bluff body flows applicable to vehicle aerodynamics. *ASME: Journal of Fluids Engineering*, 102:265–274, 1980.
2. M. Breuer. A challenging test case for the large eddy simulation: high Reynolds number circuler cylinder flow. *Int. J. Heat and Fluid Flow*, 21:648–654, 2000.
3. E. G. Duell and A. R. George. Experimental study of a ground vehicle body unsteady near wake. SAE Paper 1999-01-0812, 1999.
4. Y. I. Frucht. *High Reynolds number incompressible flow simulation about parachute canopies and similar bluff bodies.* PhD thesis, University of Leicester, 1987.
5. S. Krajnović and L. Davidson. Large eddy simulation of the flow around a ground vehicle body. In *SAE 2001 World Congress*, SAE Paper 2001-01-0702, Detroit, Michigan, USA, 2001.
6. H. Nilsson and L. Davidson. CALC-PVM: A parallel SIMPLEC multiblock solver for turbulent flow in complex domains. Int.rep. 98/12, Dept. of Thermo and Fluid Dynamics, Chalmers University of Technology, Gothenburg, 1998.
7. D. Sujudi and R. Haimes. Identification of swirling flow in 3-D vector fields. AIAA Paper AIAA 95-1715, 1995.

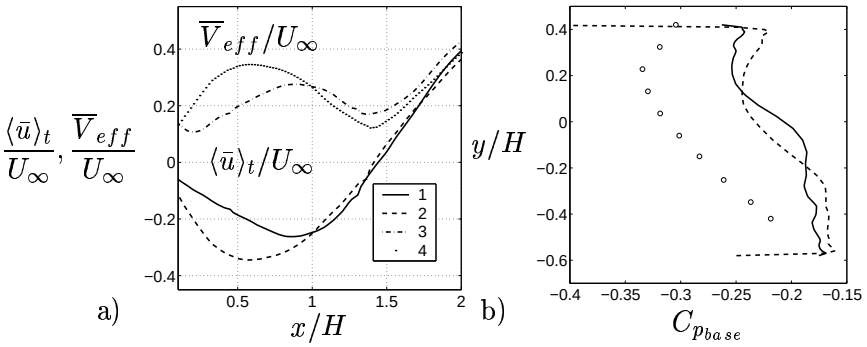

Figure 3. a) Distribution of the mean velocity component, $\langle\bar{u}\rangle_t/U_\infty$, $LES1$ (1); $LES2$ (2) and the mean velocity, $\overline{V}_{eff}/U_\infty$, $LES1$ (3); $LES2$ (4) along the x-axis at $y = 0$, $z = 0$. b) Distribution of the $C_{p_{base}}$ along the y-axis. Experimental data (symbols); $LES2$ (solid line); $LES1$ (dashed line).

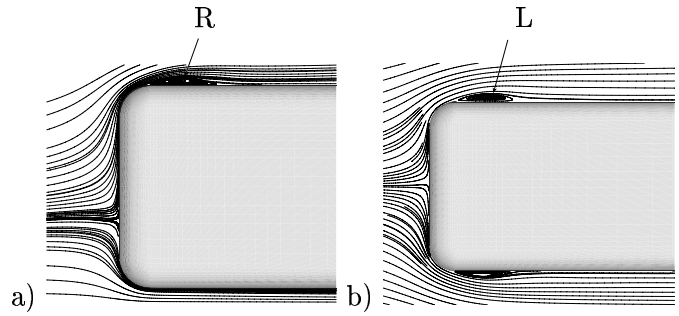

Figure 4. Simulation $LES2$. a) Time-averaged streamlines projected onto the symmetry plane, $z = 0$, of the bus. b) Time-averaged streamlines projected onto the symmetry plane, $y = 0$, of the bus.

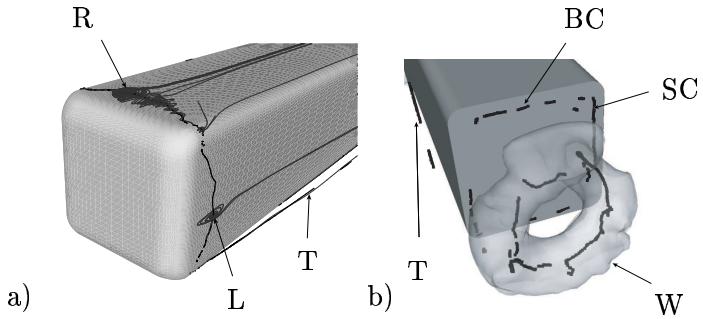

Figure 5. Simulation $LES2$. a) Streamlines emitted from the vortex cores on the roof (R), lateral sides (L) of the bus and trailing vortices (T). b) View of the rear face of the bus. The ring-type vortex (W) visualized with isosurface of pressure $p = -0.21$ and its vortex core. BC and SC are thin corner vortices behind the rear face of the model.

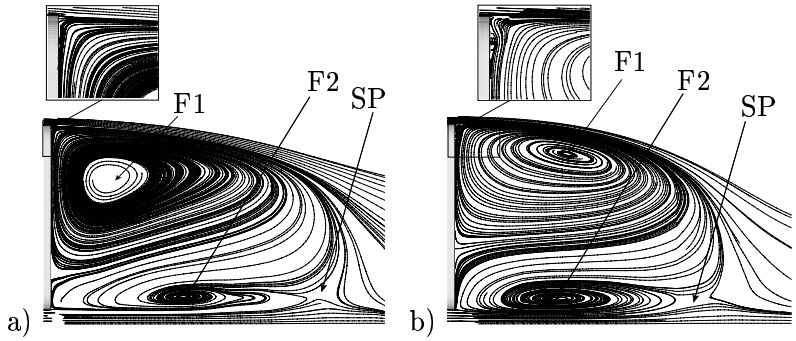

Figure 6. Time-averaged streamlines projected onto the symmetry plane, $z = 0$, of the bus. F1 and F2 are foci of vortices and SP is saddle point. a) $LES1$; b) $LES2$.

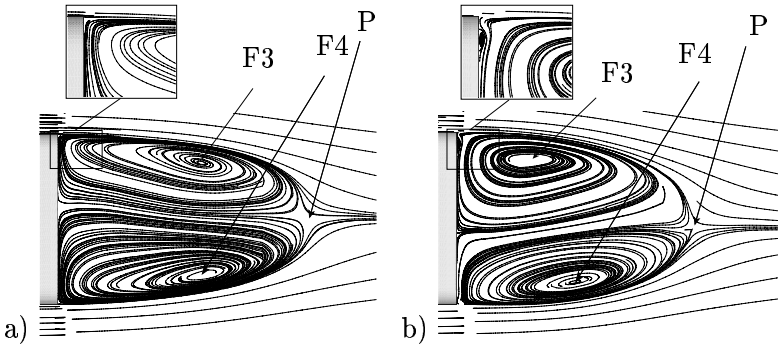

Figure 7. Time-averaged streamlines projected onto the symmetry plane, $y = 0$, of the bus. F3 and F4 are foci of vortices and P is free stagnation point. a) $LES1$; b) $LES2$.